Journal of Power Sources 260 (2014) 225–232

Contents lists available at ScienceDirect

Journal of Power Sources

journal homepage: www.elsevier.com/locate/jpowsour

Multifunctional graphene incorporated conducting gel electrolytes in enhancing photovoltaic performances of quasi-solid-state dye-sensitized solar cells

Shuangshuang Yuan, Qunwei Tang*, Benlin He, Yun Zhao

Institute of Materials Science and Engineering, Ocean University of China, 266100 Qingdao, PR China

HIGHLIGHTS

- Graphene, graphene oxide, or nanographite is incorporated into microporous PAA-CTAB matrix.
- The electrocatalytic reaction of triiodides is conducted into conducting gel electrolyte.
- Liquid electrolyte is driven by osmotic pressure and capillary diffusion.
- An efficiency of 7.06% is recorded in PAA-CTAB/graphene gel electrolyte based DSSC.

GRAPHICAL ABSTRACT

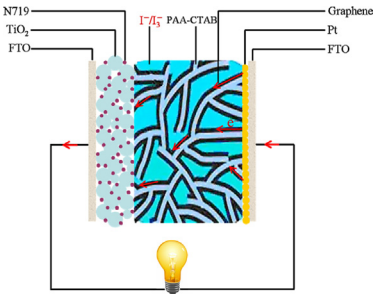

ARTICLE INFO

Article history:
Received 23 December 2013
Received in revised form
8 February 2014
Accepted 12 March 2014
Available online 19 March 2014

Keywords:
Quasi-solid-state dye-sensitized solar cell
Conducting gel electrolyte
Graphene
Amphiphilic hydrogel

ABSTRACT

Three-dimensional (3D) gel electrolytes are versatile in elevating encapsulation of liquid electrolyte in dye-sensitized solar cells (DSSCs), however, the poor contact at gel electrolyte/Pt counter electrode interface is unfavorable in electrocatalyzing triiodide ions. In the current work, we report the multifunctions of graphene, graphene oxide, or nanographite incorporated microporous poly(acrylic acid)-cetyltrimethylammonium bromide (PAA-CTAB) conducting gel electrolytes in both sealing liquid electrolyte and conducting refluxed electrons (electrons from external circuit to Pt counter electrode) into 3D framework of the conducting gel electrolyte, aiming at elevating liquid electrolyte content in per unit volume of gel electrolyte, increasing electrocatalytic area toward triiodide ions and diminishing charge-transfer resistance. The electrical and electrochemical performances of the resultant conducting gel electrolytes are thoroughly characterized. Light-to-electric power conversion efficiencies of 7.06%, 6.35%, and 6.17% are determined from DSSCs using graphene, graphene oxide, and nanographite incorporated PAA-CTAB conducting gel electrolytes in comparison with 6.07% from pure PAA-CTAB based DSSC.

1. Introduction

In nowaday low-carbon society, wide application of fossil fuels (coal, oil, and natural gas) has brought gigantic problems in energy exhaustion, environmental pollution, and ecological destruction [1,2]. Among diversiform candidates, dye-sensitized solar cell (DSSC) [3–6], electrochemical device converting solar energy directly into electricity, is one of the preferred alternatives because of its merits in relatively low fabrication cost, relatively high power conversion efficiency, and zero emission. A typical DSSC device is composing of dye-sensitized TiO_2 photoanode, electrolyte filled with redox couples, and a Pt counter electrode. Acetonitrile dissolved I^-/I_3^- solution is commonly employed as liquid electrolyte in fabricating DSSCs. Up to now, a power conversion efficiency of

* Corresponding author. Tel./fax: +86 532 66781690.
E-mail address: tangqunwei@ouc.edu.cn (Q. Tang).

http://dx.doi.org/10.1016/j.jpowsour.2014.03.034
0378-7753/

12.3% has been determined from a liquid electrolyte based DSSC [7]. The main issue of this class of DSSCs is leakage of liquid electrolyte and evaporation of organic solvent such as acetonitrile [8]. The loss of medium for redox couple transportation is expected to significantly decrease recovery of excited dye molecules. Therefore, it is a prerequisite to find stable electrolytes in storing redox species.

Polymer gel electrolytes and solid electrolytes are sustainable preferences in designing stable DSSCs [9–14]. Charge transfer in solid electrolytes is generally dependent on migration or vibration of molecular segments which is relatively low in comparison with easy flow of liquid electrolyte. The power conversion efficiencies of full-solid-state DSSCs are therefore still unsatisfactory [15,16]. To combine the stability of solid electrolytes and rapid charge transfer of liquid electrolytes, polymer gel electrolytes have been widely demonstrated, especially the gel electrolytes having three-dimensional (3D) frameworks. The diffusion of liquid electrolyte into polymer or polymer composite matrices is only governed by Flory theory accompanied with expansion in volume, in which osmotic pressure across the matrix is a driving force [17]. The imbibed liquid electrolyte can be stored in the 3D framework of gel matrix even under assembly of DSSC. There are still two remaining problems unsolved in designing efficient quasi-solid-state DSSCs: (i) relatively low liquid electrolyte in per unit volume, leading to large resistance in transferring charges; (ii) poor contact at gel electrolyte/Pt counter electrode interface, giving unreasonable electroreduction reaction of triiodides. By addressing these two issues, we pioneerly report the feasibility of microporous gel matrix in loading graphene, graphene oxide, or nanographite dissolved liquid electrolyte. Owing to the cooperative driving of osmotic pressure across the matrix and capillary force presenting in the micropores [18], increased amount of liquid electrolyte is imbibed, whereas the incorporated conducting substances are expected to attach on inner surface of gel matrix to form interconnected channels. The interfacial contact between conducting gel electrolyte and Pt counter electrolyte is also improved by conducting reflux electrons (the electrons from external circuit to Pt counter electrode) from Pt layer to 3D interconnected channels of conducting substances. Therefore, the electrocatalytic reaction of triiodides is extended from gel electrolyte/Pt interface to both interface and 3D framework of conducting gel electrolyte.

In the current work, we open an approach of designing efficient conducting gel electrolytes from incorporating graphene, graphene oxide, or nanographite dissolved liquid electrolyte with freeze-dried microporous poly(acrylic acid)-cetyltrimethylammonium bromide (PAA-CTAB). The imbibition kinetics is governed by both osmotic pressure and capillary force across the membrane and micropores. Results indicate that the electrical, electrochemical and therefore photovoltaic performances of the conducting gel electrolytes and their DSSCs have been enhanced in comparison with the electron-insulating PAA-CTAB gel electrolyte. The multifunctions of conducting materials such as graphene, graphene oxide, or nanographite in elevating the photovoltaic performances of quasi-solid-state DSSCs are demonstrated.

2. Experimental

2.1. Synthesis of PAA-CTAB matrix

PAA-CTAB matrix was synthesized by modifying the procedures: 1.0 g of CTAB and 10 g of acrylic acid were dispersed in 10 ml of deionized water. Subsequently, initiator ammonium peroxydisulfate (APS) (mass ratio of APS to acrylic acid was 0.0225) and crosslinker N,N′-methylene bisacrylamide (NMBA) (mass ratio of NMBA to acrylic acid was 0.001) were added to the mixed solution. Under a nitrogen atmosphere, the acrylic acid-CTAB monomers would be initiated by the thermal decomposition of APS for forming PAA-CTAB prepolymer. With the proceeding of polymerization, the viscosity increased gradually. When the viscosity of the PAA-CTAB prepolymers reached around 180 mPa s^{-1} (The viscosity of the reagent was measured using a Haaker ReoStress RS75 rheometer at a shear rate of around 100 s^{-1}), the reagent was poured into a petri dish and cooled to room temperature until the formation of an elastic gel. After rinsing with excess deionized water, the samples were vacuum dried at 80 °C for more than 12 h.

2.2. Synthesis of conducting gel electrolytes

The microporous PAA-CTAB matrices were prepared by immersing dried PAA-CTAB matrices in deionized water for 72 h to reach their swelling equilibrium, and subsequently freeze-dried under vacuum at −60 °C for 72 h. Later, the membranes were immersed in liquid electrolyte consisting of redox electrolyte and graphene or graphene oxide or nanographite for 10 days to reach absorption equilibrium. The content of each conducting substance (graphene, graphene oxide, or nanographite) was 1.33 g L^{-1}. A redox electrolyte consisted of 100 mM of tetraethylammonium iodide, 100 mM of tetramethylammonium iodide, 100 mM of tetrabutylammonium iodide, 100 mM of NaI, 100 mM of KI, 100 mM of LiI, 50 mM of I_2, and 500 mM of 4-tert-butyl-pyridine in 50 ml of acetonitrile.

2.3. Assembly of quasi-solid-state DSSCs

TiO_2 colloid was prepared according to the literature and a layer of TiO_2 nanocrystal anode film with a thickness of 10 μm and an area of 0.25 cm^2 was prepared by coating TiO_2 colloid onto conducting glass using a doctor blade technique, followed by sintering in air at 450 °C for 30 min. Subsequently, the TiO_2 film was soaked in a 0.3 mM N719 [cis-di(thiocyanato)-N,N′-bis(2,2′-bipyridyl-4-carboxylic acid-4-tetrabutylammonium carboxylate, purchased from Solaronix, SA, Switzerland] ethanol solution for 24 h to uptake N719 dye for the fabrication of dye-sensitized TiO_2 photoanode. Quasi-solid-state DSSC from pure PAA-CTAB, PAA-CTAB/graphene, PAA-CTAB/graphene oxide, or PAA-CTAB/nanographite gel electrolyte was fabricated by sandwiching a slice of gel electrolyte with thickness of around 500 μm between a dye-sensitized TiO_2 anode and a Pt counter electrode.

2.4. Photovoltaic measurements

The photocurrent-voltage (J–V) curves of the assembled quasi-solid-state DSSCs were recorded on an Electrochemical Workstation (CHI600E) under irradiation of a simulated solar light from a 100 W xenon-mercury arc lamp (CHF-XM-500W, Beijing Trusttech Co., Ltd) in ambient atmosphere. The incident light intensity was calibrated using an FZ-A type radiometer from Beijing Normal University Photoelectric Instrument Factory to control it at 100 mW cm^{-2} (AM 1.5). Each DSSC device was measured five times to eliminate experimental error and a compromise J–V curve was employed.

2.5. Characterizations

The morphology of the microporous PAA-CTAB matrix was captured with a Zeiss Ultra plus field emission scanning electron microscopy (FESEM). To observe the internal 3D microstructure, swollen PAA-CTAB hydrogel were first cut into ultrathin film, followed by the loading into a chamber under freezing temperature and high vacuum to remove solvent. Fourier transform infrared spectrometry (FTIR) spectra were recorded on a Vertex 70 FTIR

spectrometer (Bruker). The ionic conductivities of gel electrolytes were measured by using a pocket conductivity meter (DSSJ-308A, LeiCi Instruments). The instrument was calibrated with 0.01 M KCl aqueous solution prior to experiments. Tafel-polarization curves of the symmetrical cells were measured by CHI660E electrochemical workstation by sandwiching a slice of gel electrolyte between two identical Pt electrodes (Pt electrode/gel electrolyte/Pt electrode). The electrochemical impedance spectroscopy (EIS) was carried out using a CHI660E electrochemical workstation at a constant temperature of 20 °C with an ac signal amplitude of 20 mV in the frequency range from 0.1 to 10^5 Hz in the dark. The cyclic voltammetry (CV) was also carried out on the CHI660E electrochemical workstation in a N_2-purged liquid electrolyte: (1) gel electrolyte was used as working electrode, (2) Pt wire pierced gel electrolyte was used as working electrode by controlling the piercing depth of Pt wire into gel electrolyte at 1 cm, Pt foil as the counter electrode, and an Ag/AgCl electrode as reference electrode, the supporting electrolyte was 0.1 M $LiClO_4$ whereas the redox couple was 10 mM LiI and 1 mM I_2.

3. Results and discussion

The FTIR spectra of PAA-CTAB/graphene, PAA-CTAB/graphene oxide, PAA-CTAB/nanographite, and pure PAA-CTAB matrix are shown in Fig. 1, where the absorption bands at 1679, 1506, and 1439 cm^{-1} in pure PAA-CTAB matrix are originated from the vibrations of C═O stretching (PAA), C═O bending (PAA), and O—H distorting (PAA), respectively [19]. The appearance of band at 2992 cm^{-1} in pure PAA-CTAB matrix, attributing to CH_3—N^+ stretching indicates that CTAB, has been successfully integrated with PAA. Dovydov's splittings are observed for the CH_2 rocking (720 and 731 cm^{-1}) and scissoring (1460 and 1472 cm^{-1}) vibrations of CTAB methylene chains [20]. The detection of these splittings is connected with a fact that a packing of long-chain aliphatic compounds in PAA-CTAB matrix can be described by an orthorhombic crystal subcell. The band at 2870 cm^{-1}, corresponding to ordering of methylene chains, $(-CH_2-)_{12}$, has shifted to 2880 cm^{-1} in PAA-CTAB/graphene, PAA-CTAB/graphene oxide, and PAA-CTAB/nanographite [21]. This signal indicates that the hydrophobic interaction between methylene chains of PAA-CTAB and graphene (or graphene oxide, or nanographite) has an influence on vibration of alkyl chain.

The microporous structure of PAA-CTAB matrix is a prerequisite to imbibe enormous liquid electrolyte accompanied with graphene, graphene oxide or nanographite. From cross-sectional SEM photograph, as is shown in Fig. 2, it is apparent that freeze-dried PAA-CTAB matrix has an interconnected microporous structure because of the macrobiradical nature of crosslinker NMBA [22]. Electrostatic interaction between negatively charged acrylic acid monomers and positively charged CTA^+ ions (CTAB can ionize into a CTA^+ and a B^-) can form acrylic acid-CTAB complex monomers, resulting in the loss of partial hydrophilicity of —COOH group and presence of hydrophobicity of C13 alkyl chains. Therefore, the resultant PAA-CTAB matrix is an amphiphilic polymer with a 3D framework.

In previous reports [23,24], liquid electrolyte is generally imbibed into 3D framework of an amphiphilic matrix by directly immersing anhydrous matrix into liquid electrolyte composing of redox couples until an imbibition equilibrium. In this case, osmotic pressure across the matrix is a sole driving force. Although liquid electrolyte can be incorporated into 3D framework of gel matrix and can not leak from the system during cell assembly, the low liquid electrolyte loading in a gel electrolyte generates a large charge-transfer resistance. In addition, the electrochemical reaction of I^-/I_3^- redox couples between FTO layer and gel electrolyte can be restricted by the poor contact of encapsulated I^-/I_3^- redox species and FTO. The goals of our current work are to open a strategy of enhancing charge-transfer kinetics and conducting reflux electrons from Pt counter electrode to 3D PAA-CTAB framework. A synergistic effect of osmotic pressure across PAA-CTAB matrix and capillary force presenting in micropores can drive more liquid electrolyte and conducting substances such as graphene, graphene oxide, or nanographite into interconnected micropores. It is noteworthy to demonstrate that the imbibed conducting substances can form interconnected channels within a gel electrolyte, which has been confirmed in our previous research [25,26]. Once such conducting gel electrolyte is assembled into a DSSC device, the conducting channel formed by graphene, graphene oxide, or nanographite can conduct reflux electrons from Pt electrode to the whole gel electrolyte. Therefore, the conducting gel electrolyte plays three roles in its quasi-solid-state DSSC: (i) encapsulating liquid electrolyte, (ii) conducting electrons from Pt layer to 3D gel electrolyte, and (iii) electroreducing I^-/I_3^- redox species. Take the DSSC from PAA-CTAB/graphene gel electrolyte as an example, as is shown in Fig. 3, reflux electrons can be conducted from Pt layer to 3D PAA-CTAB/graphene framework along conducting channel formed by graphene nanostructures, in which I^-/I_3^- redox couples are also encapsulated. In a sense of functions, the PAA-CTAB/graphene gel electrolyte may be considered as an extension of Pt counter electrode because it can catalyze triiodides

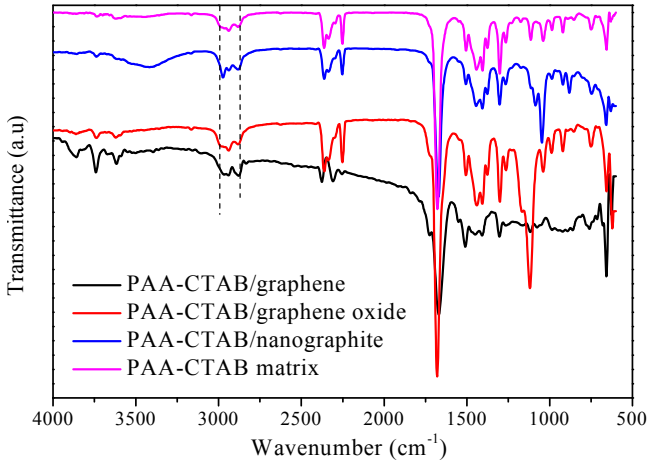

Fig. 1. FTIR spectra of PAA-CTAB/graphene, PAA-CTAB/graphene oxide, PAA-CTAB/nanographite, and PAA-CTAB matrix.

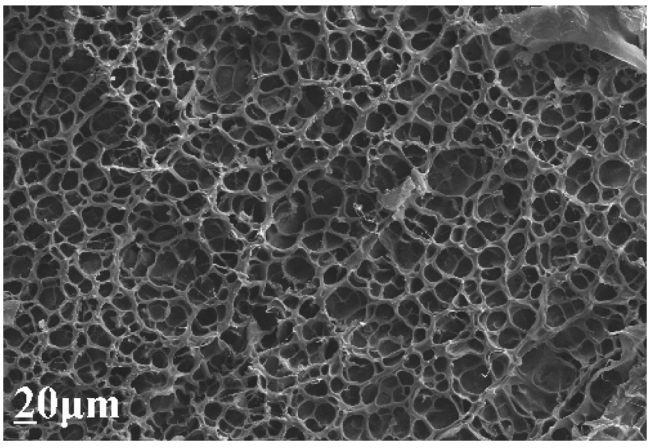

Fig. 2. Cross-sectional SEM photograph of microporous PAA-CTAB matrix.

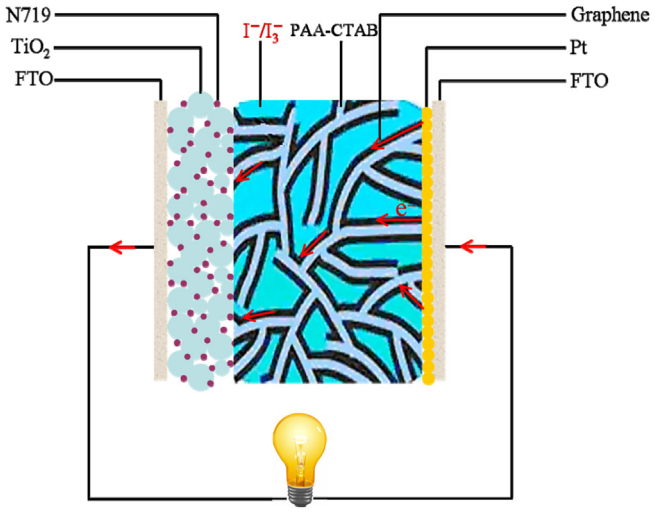

Fig. 3. Schematic diagram of a DSSC device from PAA-CTAB/graphene (or PAA-CTAB/graphene oxide or PAA-CTAB/nanographite) gel electrolyte. The transportation of reflux electrons along conducting channel within PAA-CTAB/graphene gel electrolyte is marked.

into iodides. The significant enhancements in conducting electrons and redox reaction area are expected to dramatically elevate the charge-transfer kinetics and exchange of I^-/I_3^- redox species.

The time dependences of liquid electrolyte loading and room-temperature ionic conductivity of PAA-CTAB/graphene, PAA-CTAB/graphene oxide, and PAA-CTAB/nanographite gel electrolytes are displayed in Fig. 4. As a reference, the same measurements for pure PAA-CTAB gel electrolyte are also carried out. Under a synergistic driving by osmotic pressure and capillary force, a rapid increase in liquid electrolyte loading is detected in initial stage (0–7 days) by weighing the gel electrolyte [27]. With diffusion of liquid electrolyte into PAA-CTAB matrix, the osmotic pressure and capillary force gradually decline until an imbibition equilibrium at around 12 days. It is reasonable that room-temperature ionic conductivity has a similar trend to liquid electrolyte loading because of increase of I^-/I_3^- redox species in unit volume of polymer gel electrolyte. In order to determine the imbibition kinetics of microporous PAA-CTAB matrix, the accumulative liquid electrolyte loading over time is fitted by Fickian theory [28]:

$$\frac{M_t}{M_\infty} = kt^n \tag{1}$$

where M_t and M_∞ are the masses of the imbibed liquid electrolyte at time t and at equilibrium, respectively. k is a characteristic rate constant relating to the properties of PAA-CTAB matrix, and n is a transport number characterizing the transport mechanism. $n \leq 0.5$ suggests a Fickian or Case I transport behavior in which the PAA-CTAB relaxation is much faster than the diffusion; $n = 1$ gives a non-Fickian or Case II mode of transport where liquid electrolyte uptake is controlled by diffusion process. $0.5 < n < 1$ refers to an anomalous or a Case III mode in which structural relaxation is comparable to diffusion. By plotting $\log(M_t/M_\infty)$ vs $\log(t)$, the n values are recorded and shown in inserts of Fig. 4. The n values from the microporous PAA-CTAB/graphene, PAA-CTAB/graphene oxide, PAA-CTAB/nanographite, and pure PAA-CTAB matrix are 0.64, 0.63, 0.62, and 0.77, respectively. This result indicates an anomalous mechanism mode in which structural relaxation is comparable to diffusion. Moreover, the loading of liquid electrolyte is mainly controlled by osmotic pressure.

The liquid electrolyte loading can be obtained by calculating:

$$\text{Liquid electrolyte loading}\left(g \cdot g^{-1}\right) = \frac{M_{\text{gel}} - M_{\text{polymer}}}{M_{\text{polymer}}} \tag{2}$$

where M_{gel} (g) and M_{polymer} are masses of anhydrous PAA-CTAB matrix and polymer gel electrolyte, respectively. Apparently, the PAA-CTAB/graphene has a liquid electrolyte loading of 14.1 g g^{-1}, which is much higher than 13.1 g g^{-1} for PAA-CTAB/graphene oxide, 11.4 g g^{-1} for PAA-CTAB/nanographite, and 6.73 g g^{-1} for PAA-CTAB matrix. Higher liquid electrolyte loading is expected to give a better ionic conductivity owing to a higher liquid electrolyte content in per unit volume. Room-temperature ionic conductivities of PAA-CTAB/graphene, PAA-CTAB/graphene oxide, PAA-CTAB/nanographite, and pure PAA-CTAB gel electrolytes are 10.56, 9.91, 7.33, and 6.78 mS cm^{-1}, respectively.

The ionic conductivity–temperature plots of various gel electrolytes follow an Arrhenius relationship reasonably well [29], as shown in Fig. 5. Apparently, the room-temperature ionic conductivities of the gel electrolytes are in an order of PAA-CTAB/graphene (10.56 mS cm^{-1}) > PAA-CTAB/graphene oxide (9.91 mS cm^{-1}) > PAA-CTAB/nanographite (7.36 mS cm^{-1}) > pure PAA-CTAB (6.05 mS cm^{-1}). According to Fig. 5, the activation energy values, E_a, are 6.15, 6.40, 6.98, and 7.28 kJ mol^{-1} for PAA-CTAB/graphene, PAA-CTAB/graphene oxide, PAA-CTAB/nanographite, and pure PAA-CTAB, respectively. The much lower E_a at PAA-CTAB/graphene gel electrolyte suggests an easy charge transfer process [30]. The increased ionic conductivity is expected to significantly enhance the reaction kinetics of DSSCs.

Fig. 6(a) shows the CV curves recorded using PAA-CTAB/graphene, PAA-CTAB/graphene oxide, PAA-CTAB/nanographite, or PAA-CTAB gel electrolyte as working electrolyte, Ag/AgCl as a reference electrode, Pt foil as a counter electrode, and liquid electrolyte as supporting electrolyte. No redox peaks are observed using pure PAA-CTAB gel electrolyte as working electrode, indicating no electrocatalytic activity of PAA-CTAB to I^-/I_3^- redox couples. Surprisingly, a pair of redox peaks are determined from PAA-CTAB/graphene, PAA-CTAB/graphene oxide, or PAA-CTAB/nanographite conducting gel electrolyte, suggesting that the conducting gel electrolytes have electrocatalytic activity toward I^-/I_3^- redox species. The peak positions and shapes of the CV curves are very similar to those of graphene, graphene oxide, or nanographite counter electrode [31–33]. It is well known that a counter electrode in a DSSC device is a mediator in conducting reflux electrons and reducing I_3^- ions, therefore, graphene, graphene oxide, and nanographite have been widely employed as non-Pt counter electrode materials for DSSCs. Among two pairs of redox reaction, $I^- \leftrightarrow I_3^-$ is dominant in controlling the whole reaction kinetics, therefore, the peak current density of Red_1 can be used to assess the electrocatalytic activity of conducting gel electrolyte. PAA-CTAB/graphene gel electrolyte has the highest current density, suggesting the best electrocatalytic performance. After careful analysis, we can make a conclusion that the incorporated conducting substances such as graphene, graphene oxide, or nanographite can form interconnected channels for electron conduction and catalytic reaction. The diffusion kinetics of triiodides in the 3D framework of conducting gel electrolyte is significant for accelerating recovery of redox couples, this process can be evaluated by Randles-Sevcik theory [34]:

$$J_{\text{red1}} = Kn^{1.5}ACD_n^{0.5}v^{0.5}$$

where J_{red1} is the peak current density of Red_1 (mA cm^{-2}), K is 2.69×10^5, n is the number of electrons of reduction reaction, A is the electrode area (cm^2), C represents the bulk concentration of I_3^- (mol L^{-1}), D_n is the diffusion coefficient (cm^{-2} s^{-1}). The D_n of PAA-

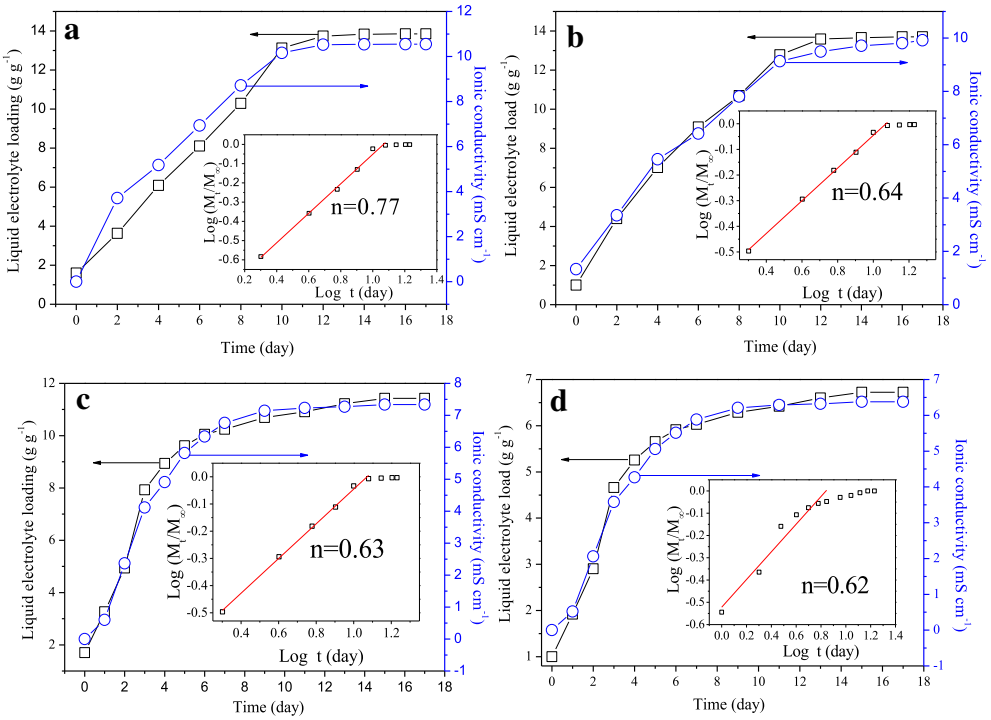

Fig. 4. Time dependences of liquid electrolyte loading and ionic conductivity for (a) PAA-CTAB, (b) PAA-CTAB/graphene, (c) PAA-CTAB/graphene oxide, and (d) PAA-CTAB/nanographite gel electrolytes.

CTAB/graphene, PAA-CTAB/graphene oxide, and PAA-CTAB/nanographite gel electrolytes are 1.29×10^{-5}, 1.39×10^{-5}, and 1.55×10^{-5} cm^{-2} s^{-1}, respectively, which are larger than 2.55×10^{-6} cm^{-2} s^{-1} for pure Pt counter electrode [35]. Results indicate that the conducting gel electrolytes have good electrocatalytic activities toward I^-/I_3^- redox species.

Two pairs of redox peaks are observed in each CV curve by piercing a Pt wire into gel electrolyte. As is shown in Fig. 6(b), the redox reactions are attributed to the synergistic effect of Pt wire and conducting channels from graphene, graphene oxide or nanographite in gel electrolyte toward I^-/I_3^- redox species. The electrocatalytic performances can also be assessed by comparing the peak current density for Red_1. The electrocatalytic functions of

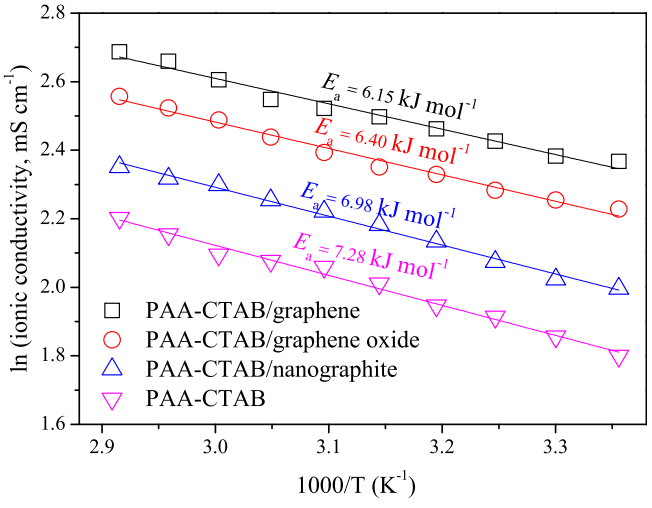

Fig. 5. Arrhenius plots of various gel electrolytes: (a) PAA-CTAB/graphene, (b) PAA-CTAB/graphene oxide, (c) PAA-CTAB/nanographite, and (d) PAA-CTAB.

Pt wire are believed to be similar because of the same piercing dept of Pt wire in gel electrolytes. Therefore, the electrocatalytic activity follows an order of PAA-CTAB/graphene > PAA-CTAB/graphene oxide > PAA-CTAB/nanographite, which is in an agreement with result of Fig. 6(a).

From the stacking CV curves of conducting gel electrolytes at different scan rates, one can find an outward extension of all the peaks (Fig. 7(a)–(c)). By plotting peak current density corresponding to $I_3^- \leftrightarrow I^-$ versus square root of scan rate, as shown in Fig. 7(d), linear relationships are observed. This result indicates the redox reaction is a diffusion-controlled mechanism on PAA-CTAB/graphene, PAA-CTAB/graphene oxide, and PAA-CTAB/nanographite gel electrolytes [36].

Nyquist plots in Fig. 8(a) illustrate impedance characteristics of a symmetric cell fabricated by sandwiching a conducting gel electrolyte slice between two Pt counter electrodes. According to the Randles-type circuit (inset of Fig. 8(a)), the intercept on the real axis represents the series resistance (R_s), that is the resistance of Pt counter electrode. The arc arises from the charge-transfer resistance (R_{ct}) at Pt counter electrode/gel electrolyte interface, which changes inversely with the electrocatalytic activity of CEs on the reduction of triiodide, whereas W represents the Nernst diffusion impedance corresponding to the diffusion resistance of I^-/I_3^- redox species. CPE is a constant phase element and is frequently used as a substitute for a capacitor in an equivalent circuit to fit the impedance behavior of the electrical double layer. All the EIS plots have a similar R_s value because the same Pt counter electrode was used in assembling the symmetric cells. R_{ct} decreases in an order of PAA-CTAB/graphene < PAA-CTAB/graphene oxide < PAA-CTAB/nanographite, indicating an inverse order of electrocatalytic activity. The conclusions for the electrocatalytic activity and diffusion derived from EIS and CV data are consistent. Tafel-polarization plots were also recorded to determine the electrocatalytic activity of the gel electrolytes, which was also performed with an asymmetric similar to those used in EIS measurements, are shown in Fig. 8(b). A larger

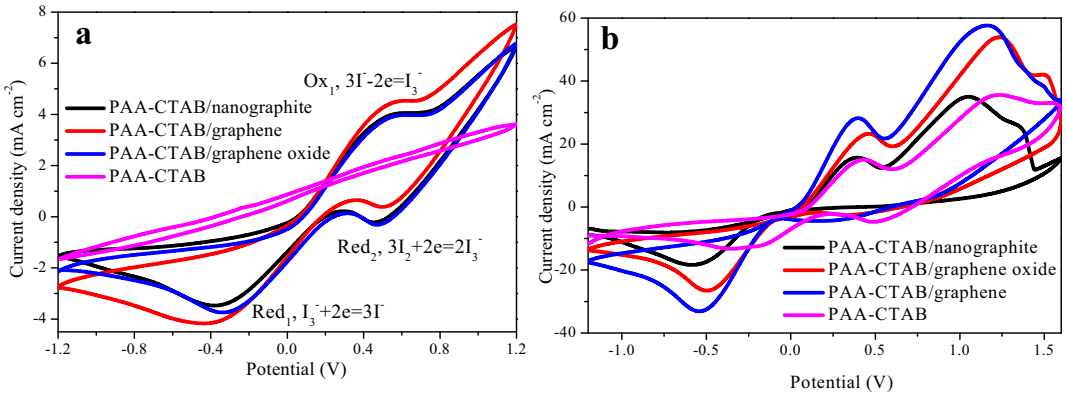

Fig. 6. (a) CV curves recorded using gel electrolyte as working electrodes. The active area of each gel electrolyte slice was 1 cm^2. (b) CV curves obtained from piercing a Pt wire in gel electrolytes. The active area of gel electrolytes was 2 cm^2 and the length of Pt wire in a gel electrolyte was 0.5 cm. All the curves were scanned at a scan rate of 50 mV s^{-1}.

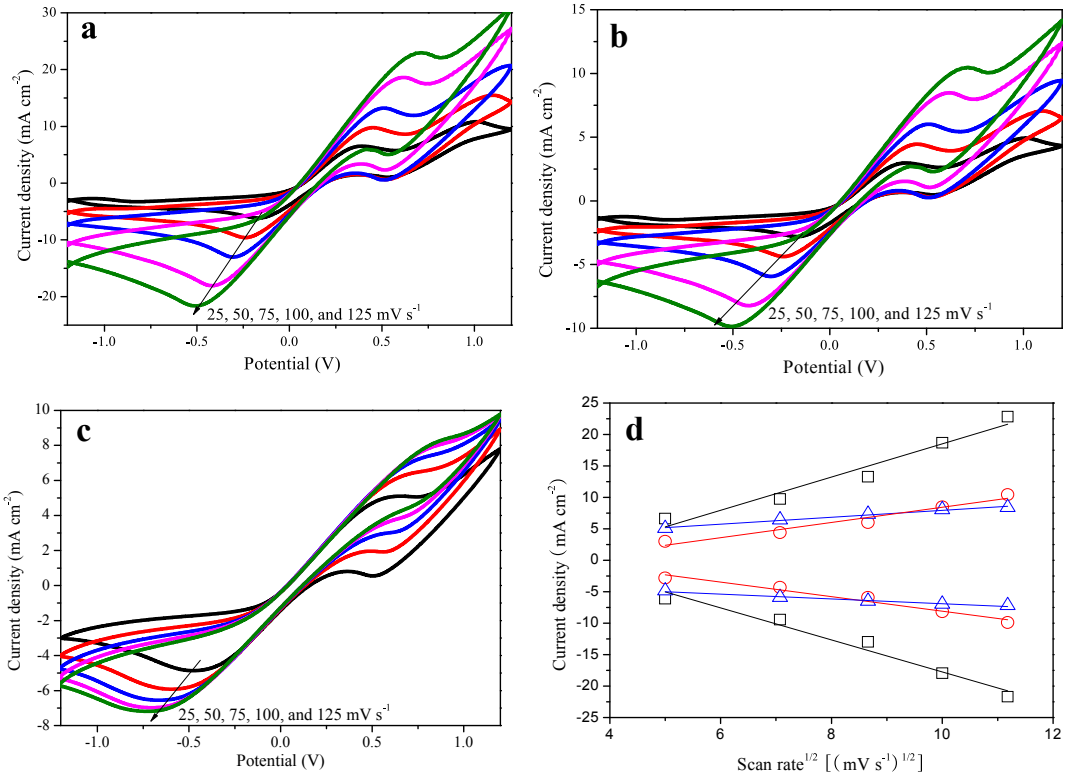

Fig. 7. CV curves of (a) PAA-CTAB/graphene, (b) PAA-CTAB/graphene oxide, and (c) PAA-CTAB/nanographite gel electrolytes for I^-/I_3^- redox species at varied scan rates (from inner to outer: 25, 50, 75, 100, and 125 mV s^{-1}), and (d) relationship between peak current densities and square root of scan rates: (Square) PAA-CTAB/graphene, (Circle) PAA-CTAB/graphene oxide, (Uptriangle) PAA-CTAB/nanographite. All CV curves were recorded using gel electrolyte as working electrodes. The active area of each gel electrolyte slice was 1 cm^2.

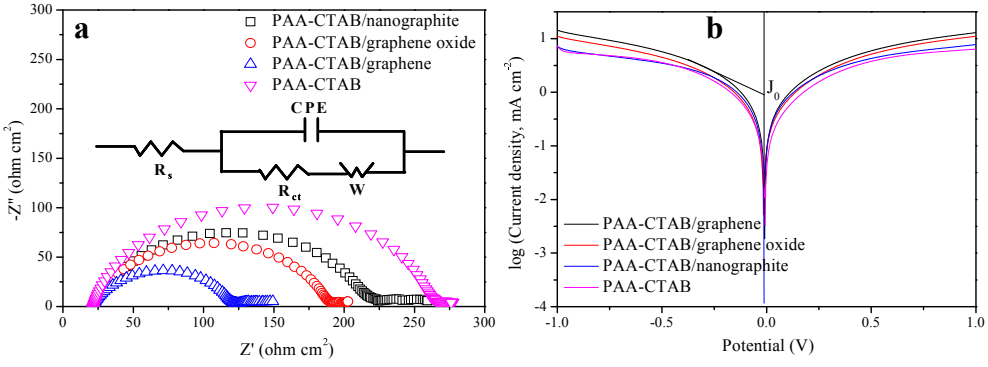

Fig. 8. (a) Nyquist plots and (b) Tafel polarization curves for symmetric cells fabricated by sandwiching a conducting gel electrolyte slice between two Pt counter electrodes.

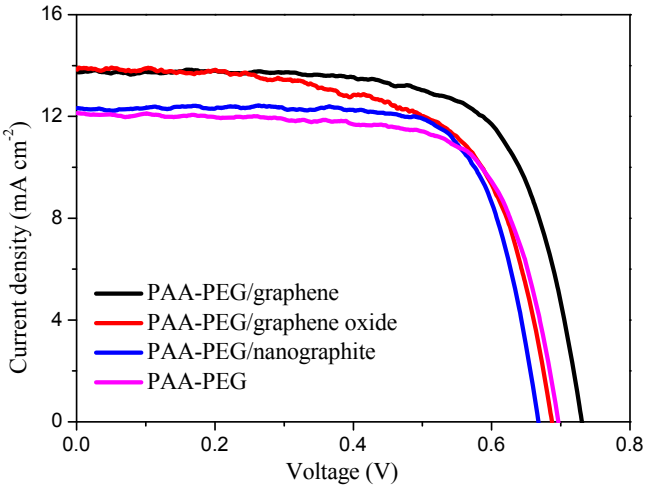

Fig. 9. *J–V* characteristics of DSSCs from PAA-CTAB/grapheme, PAA-CTAB/graphene oxide, PAA-CTAB/nanographite, and PAA-CTAB gel electrolytes.

slope in the anodic or cathodic branch indicates a higher exchange current density (J_0) and better electrocatalytic activity toward redox couples on the gel electrolytes. It is obvious that the J_0 value is in an order of PAA-CTAB/graphene > PAA-CTAB/graphene oxide > PAA-CTAB/nanographite > PAA-CTAB, which is consistent with R_{ct} in EIS spectra.

Fig. 9 shows the photovoltaic characteristics of DSSCs from various gel electrolytes and the parameters reflecting DSSC properties are summarized in Table 1. A power conversion efficiency of 6.07% is recorded from PAA-CTAB gel electrolyte based DSSC under solar irradiation of 100 mW cm^{-2}, which is in the same level of literatures [37,38]. However, the efficiency has been significantly enhanced by incorporating graphene, graphene oxide, or nanographite into PAA-CTAB matrix, and an efficiency of 7.06% is recorded on the DSSC from PAA-CTAB/graphene gel electrolyte. To eliminate the experimental error, each experiment has been repeated five times and a compromise curve is employed. As mentioned above, the combination of graphene, graphene oxide, or nanographite with PAA-CTAB matrix is expected to accelerate the recovery of redox couples. Therefore, the recovered redox couples can rapidly participate in the reduction reaction of excited dye, resulting in an elevation of photocurrent. In addition, the electrocatalysis of conducting gel electrolytes toward I^-/I_3^- redox in the 3D framework of gel electrolyte decreases the overpotential and enhanced V_{oc}. Therefore, the quasi-solid-state DSSCs from conducting gel electrolyte have predominant photovoltaic performances.

4. Conclusions

In summary, microporous PAA-CTAB matrix has been successfully synthesized and employed as placeholder for graphene (or graphene oxide or nanographite) and liquid electrolyte loading. The incorporated conducting substances (such as graphene, graphene oxide, and nanographite) combine with 3D framework of PAA-CTAB matrix by hydrophobic interaction and form interconnected channels for charge transfer. Compared with pure PAA-CTAB gel electrolyte, the liquid electrolyte loading and therefore ionic conductivity have been significantly enhanced because of increase of liquid electrolyte content in per unit volume. The interconnected channels from graphene, graphene oxide, or nanographite in conducting gel electrolyte can conduct reflux electrons from Pt counter electrode into its 3D framework and participate in the electrocatalytic reaction of I^-/I_3^- redox species. Quasi-solid-state DSSC from PAA-CTAB/graphene gel electrolyte gives a power conversion efficiency of 7.06% in comparison with 6.07% from pure PAA-CTAB based DSSC device. This research opens a gateway to improve the photovoltaic performances of quasi-solid-state DSSCs and highlights competitive capacity of the quasi-solid-state DSSCs among photovoltaic devices. The research presented here is far from being optimized but these profound advantages along with low-cost synthesis and scalable materials promise the new PAA-CTAB/graphene gel electrolyte to be strong candidates in efficient quasi-solid-state DSSCs.

Table 1
Comparison of short-circuit current density (J_{sc}), open-circuit voltage (V_{oc}), fill factor (FF), and power conversion efficiency (η) in the resultant DSSCs.

Gel electrolytes	Photovoltaic parameters			
	J_{sc} (mA cm^{-2})	V_{oc} (mV)	FF	η (%)
PAA-CTAB	12.15	696	0.718	6.07
PAA-CTAB/graphene	13.83	731	0.698	7.06
PAA-CTAB/graphene oxide	13.74	687	0.627	6.35
PAA-CTAB/nanographite	12.30	669	0.750	6.17

Acknowledgements

The authors gratefully acknowledge Ocean University of China for providing Seed Fund to this project, and Fundamental Research Funds for the Central Universities (201313001, 201312005), Shandong Province Outstanding Youth Scientist Foundation Plan (BS2013CL015), Doctoral Fund of Ministry of Education of China (20130132120023), Shandong Provincial Natural Science Foundation (ZR2011BQ017), and Research Project for the Application Foundation in Qingdao (13-1-4-198-jch).

References

[1] S. Yoda, K. Ishihara, J. Power Sources 68 (1997) 3–7.
[2] C. Okkerse, H. van Bekku, Green. Chem. 1 (1999) 107–114.
[3] B. O'Regan, M. Grätzel, Nature 353 (1991) 737–740.
[4] M. Grätzel, Nature 414 (2001) 338–344.
[5] U. Bach, D. Lupo, P. Comte, J.E. Moser, F. Weissortel, J. Salbeck, et al., Nature 395 (1998) 583–585.
[6] E.J.W. Crossland, N. Noel, V. Sivaram, T. Leijtens, J.A. Alexander-Webber, H.J. Snaith, Nature 495 (2013) 215–220.
[7] A. Yella, H.W. Lee, H.N. Tsao, C. Yi, A.K. Chandiran, M.K. Nazeeruddin, et al., Science 334 (2011) 629–634.
[8] K.F. Chen, C.H. Liu, C.K. Hsieh, C.L. Lin, H.K. Huang, C.H. Tsai, et al., J. Power Sources 247 (2014) 939–946.
[9] Q.H. Li, Q.W. Tang, N. Du, Y. Qin, J. Xiao, B.L. He, et al., J. Power Sources 248 (2014) 816–821.
[10] Q.H. Li, X.X. Chen, Q.W. Tang, H.Y. Cai, Y. Qin, B.L. He, et al., J. Power Sources 248 (2014) 923–930.
[11] Q.H. Li, H.Y. Chen, L. Lin, P.J. Li, Y.C. Qin, M.J. Li, et al., J. Mater. Chem. A 1 (2013) 5326–5332.
[12] Q.H. Li, X.X. Chen, Q.W. Tang, H.T. Xu, B.L. He, Y.C. Qin, J. Mater. Chem. A 1 (2013) 8055–8060.
[13] C.P. Lee, L.Y. Lin, R. Vittal, K.C. Ho, J. Power Sources 196 (2011) 1665–1670.
[14] Z. Huo, C. Zhang, X. Fang, M. Cai, S.Y. Dai, K. Wang, J. Power Sources 195 (2010) 4384–4390.
[15] C.P. Lee, M.H. Yeh, R. Vittal, K.C. Ho, J. Mater. Chem. 21 (2011) 15471–15478.
[16] C.L. Chen, T.W. Chang, S.C. Su, H. Teng, Y.L. Lee, J. Power Sources 247 (2014) 406–411.
[17] S.S. Yuan, Q.W. Tang, B.L. He, H.Y. Chen, Q.H. Li, C.Q. Ma, et al., J. Power Sources 249 (2014) 277–284.
[18] Q.W. Tang, S.S. Yuan, H.Y. Cai, J. Mater. Chem. A 1 (2013) 630–636.
[19] Q.W. Tang, J.H. Wu, J.M. Lin, Q.H. Li, S.J. Fan, J. Mater. Sci. 43 (2008) 5884–5890.
[20] T. Bezrodna, G. Puchkovska, V. Styopkin, J. Baran, Thin Solid Films 517 (2009) 1759–1764.
[21] X. Dang, C. Hu, D. Shen, Z. Chen, S. Hu, J. Electroanal. Chem. 657 (2011) 39–45.
[22] J.M. Lin, Q.W. Tang, D. Hu, X.M. Sun, Q.H. Li, J.H. Wu, Colloid. Surf. A 346 (2009) 177–183.
[23] J.H. Wu, Z. Lan, J.M. Lin, M.L. Huang, S.C. Hao, T. Sato, et al., Adv. Mater. 19 (2007) 4006–4011.

[24] Z. Lan, J.H. Wu, S.C. Hao, J.M. Lin, M.L. Huang, Energy Environ. Sci. 2 (2009) 524–528.
[25] J.M. Lin, Q.W. Tang, J.H. Wu, S.C. Hao, React. Funct. Polym. 67 (2007) 275–281.
[26] J.M. Lin, Q.W. Tang, J.H. Wu, React. Funct. Polym. 67 (2007) 489–494.
[27] J.H. Wu, Y.L. Wei, J.M. Lin, S.B. Lin, Polymer 44 (2003) 6513–6520.
[28] N.W. Franson, N.A. Peppas, J. Appl. Polym. Sci. 28 (1983) 1299–1310.
[29] Q.W. Tang, Y. Li, Z.Y. Tang, J.H. Wu, J.M. Lin, M.L. Huang, J. Mater. Chem. 21 (2011) 16010–16017.
[30] Q.W. Tang, K. Huang, G.Q. Qian, B.C. Benicewicz, J. Power Sources 229 (2013) 36–41.
[31] K. Yu, Z. Wen, H. Pu, G. Lu, Z. Bo, H. Kim, et al., J. Mater. Chem. A 1 (2013) 188–193.
[32] H.S. Jang, J.M. Yun, D.Y. Kim, D.W. Park, S.I. Na, S.S. Kim, Electrochim. Acta 81 (2012) 301–307.
[33] G. Veerappan, W. Kwon, S.W. Rhee, J. Power Sources 196 (2011) 10798–10805.
[34] Y.M. Xiao, J.Y. Lin, S.Y. Tai, S.W. Chou, G.T. Yue, J.H. Wu, J. Mater. Chem. 22 (2012) 19919–19925.
[35] J.Y. Lin, J.H. Liao, J. Electrochem. Soc. 159 (2012) D65–D71.
[36] Z. Lv, J. Yu, H. Wu, J. Shang, D. Wang, S. Hou, et al., Nanoscale 4 (2012) 1248–1253.
[37] Y. G. Zhang, J. Zhao, B. Q. Sun, X. J. Chen, Q. Li, L. Qiu, et al, 61 (2012) 185–190.
[38] Y. Cui, J. Zhang, X. Zhang, J. Feng, Y. Hong, Y. Zhu, Org. Electron 13 (2012) 2561–2567.